

1. Supplementary Information for the Materials & Methods Section

Selected parameters (MC Core, MC Coating, Cell Source, Cell Culture Medium Type, Biodegradability) from several studies to cultivate human cells are summarized in this table. None of these studies, except our with MC *BR44*, concerns the combination of PLGA / gelatin MCs, human cells, and defined xeno- and serum-free medium. Corning's Dissolvable MC is made of a natural biopolymer that can be dissolved at the end of the cell culture process, eliminating the mandatory cells/MCs separation step, leading to cell losses and reduced viability of the harvested population. Cytodex 1, Cytodex 3, and Cultisphere S were also used in some studies as dissolvable MCs for cell culture.

Meaning of the abbreviations and the acronyms used in the table: PLGA: poly-lactic-*co*-glycolic acid; PCL: poly- ϵ -caprolactone; PGA: poly-glycolic acid; P_{D,L}LGA: Poly-*dl*-lactic-*co*-glycolic acid; hTERT: human telomerase reverse transcriptase immortalized cells; ASC: Adipose Stem Cells; BM-MS: Bone Marrow-derived Mesenchymal Stem Cells; UC-MS: Umbilical cord-derived Mesenchymal Stem Cells; WJ-MS: Wharton's Jelly-derived Mesenchymal Stem Cells; iPS: Induced Pluripotent Stem Cells; ESC: Embryonic Stem Cells; FBS: medium contain Fetal Bovine Serum

Table S1. Published case studies for culture systems for human cells based on dissolvable or biodegradable microcarriers.

MC Name/Code	MC Core	MC Coating	Cell Source	Medium Type	Biodegradable
<i>BR44</i>	PLGA	Porcine Gelatine	hTERT ASC	Chemically Defined	YES
Fujifilm Cellnest™ Macroporous [1]	Collagen I	None	BM-MS	FBS	YES
3D Table Trix [2]	Gelatin	None	ASC UC-MS	FBS, Serum-Free, Chemically defined	YES
Corning Dissolvable [3]	PGA	Collagen/ Synthemax II	iPS	Serum-Free	NO
Cultisphere G-S [4–7]	Gelatine	None	ASC BM-MS	FBS, Serum-Free	YES
PCL MC #1 [8,9]	PCL	Fibronectin / Poly-L-Lysine	BM-MS UC-MS	FBS	YES
PCL MC2 #2 [10,11]	PCL	Fibronectin / Poly-L-Lysine	ESC WJ-MS	FBS, Serum-Free	YES
PLGA/PEI MC [12]	PLGA +PEI	None	BM-MS	FBS	YES
ProNectin-F [13]	Polystyrene	Recombinant RGD	BM-MS	FBS, Chemically defined	NO
Cytodex3 [6,14]	Dextran	Type I Porcine Gelatine	ASC BM-MS UC-MS	Serum-Free	NO
P _{D,L} LGA MC [15]	P _{D,L} LGA	Gelatine Methac- rylate	hTERT BM-MS	FBS	YES

Table S2. Materials.

Name	# Catalog	Company
Phenol	327125000	Acros Organics
Ammonium hydrogen carbonate	A3689,0500	Applichem
CD61-PE	IM3605	Beckman & Coulter
CytoFLEX Daily QC Fluorospheres	B53230	Beckman & Coulter
VersaComp Antibody Capture Bead Kit	B22804	Beckman & Coulter
VersaLyse Lysing Solution	B59266AA	Beckman & Coulter
7-AAD	559925	Becton Dickinson
CD15-FITC	332778	Becton Dickinson
CD34-BV650	343624	BioLegend
CD45-PC7	304016	BioLegend
CD73-FITC	344016	BioLegend
CD105-PE	323206	BioLegend
Sso Advanced Universal SYBR Green Super-mix	1725271	Biorad
Mix-n- Stain CF®633 Labelling kit	92237	Biotium
Albumin CSL 20%	22918180119611	CLS Behring
Poly(D,L-lactide-co-glycolide) PLGA	1840421	Corbion Purac
Ultra-Low 24 well	3473	Corning
Eppendorf Tubes® 5.0 ml	0030119380	Eppendorf
85% Glycerol solution	07-3800-07	Hänseler AG
µ-Dish	81156	Ibidi
Syringe Filters	FPE-204-030	Jet Biofil
IRDye®800CW Streptavidin	926-32230	Li-Cor
Nucleospin RNA kit	740955.250	Macherey-Nagel
Polyvinyl alcohol	81381	Merck
Methylene chloride	1.06044.2500	Merck
CD34-PE	130-081-002	Miltenyi
CD36-APC	130-095-475	Miltenyi
CD90-FITC	130-095-403	Miltenyi
CD146-PE	130-092-853	Miltenyi
ProNectin-F	Z37866-6	Pall SoloHill
Microtube mesh 40 µm	43-10040-60	PluriSelect life science
GoScript Reverse Transcription System	A5001	Promega
Proteome Profiler Human Adipokine Array Kit	ARY024	R&D Systems
Citric Acid Monohydrate	C1909	Sigma-Aldrich
DAPI	D9542	Sigma-Aldrich
Ethanol	51976	Sigma-Aldrich
Formaldehyde	47608	Sigma-Aldrich
Glutaraldehyde	G6257	Sigma-Aldrich
Guanidine Thiocyanate	50980	Sigma-Aldrich
SDS	74255	Sigma-Aldrich
Sodium Chloride	S7653	Sigma-Aldrich
Triton X-100	X100	Sigma-Aldrich
Urea	U5378	Sigma-Aldrich
SYTO™40 blue fluorescent nucleic acid stain	S11351	Thermo Fisher
Trypan Blue	15250-061	Thermo Fisher
TrypLE Select	12563-029	Thermo Fisher
T25 Flask	90026	TPP
Collagenase Type B AOF	LS004147	Worthington Biochemical Corp.

Table S3. Reverse transcription detailed procedure.

Reagent	Amount
	Mix 1:
RNA	Up to 2 µg
Oligo dT	0.5 µg
Random Primers	0.5 µg
H ₂ O	Final volume: 5.0 µL
	Mix 2:
Buffer 5x	2.0 µL
MgCl ₂	1.0 µL [2.5 mM]
dNTPs	0.5 µL [0.5 mM]
Inhibitor RNase	0.25 µL [20 Units]
RT Enzyme	0.5 µL
H ₂ O	Final volume: 5.0 µL
Procedure:	
	Add Mix 1: incubate 5' at 70 °C, cool to 10 °C, and incubate 5' in ice
	Add Mix 2: incubate 5' at 25 °C, 42 °C for 1h, and 70 °C for 15'.

Table S4. Primer sequences.

Gene Name	Forward Primer (5'-3')	Reverse Primer (5'-3')
<i>ACTB</i>	CTG GAA CGG TGA AGG TGA CA	AAG GGA CTT CCT GTA ACA ATG CA
<i>SOX9</i> *	AGC GAA CGC ACA TCA AGA C	CTG TAG GCG ATC TGT TGG GG
<i>RUNX2</i> *	TCA ACG ATC TGA GAT TTG TGG G	GGG GAG GAT TTG TGA AGA CGG
<i>PPARG</i> [16]	TGA CAG CGA CTT GGC AAT ATT TAT T	TTG TAG CAG GTT GTC TTG AAT GTC T
<i>PREF1</i> *	TGA CCA GTG CGT GAC CTC T	GGC AGT CCT TTC CCG AGT A
<i>ZFP423</i> [16]	GAT CAC TGT CAG CAG GAC TT	TGC CTC TTC AAG TAG CTC A
<i>ZFP521</i> [16]	GGC TGT TCA AAC ACA AGC G	GCA CAT TTA TAT GGC TTG TTG
<i>WISP2</i> *	GCG ACC AAC TCC ACG TCT G	TCC CCT TCC CGA TAC AGG C
<i>DKK1</i> *	ATA GCA CCT TGG ATG GGT ATT CC	CTG ATG ACC GGA GAC AAA CAG

* Primer from PrimerBank (<https://pga.mgh.harvard.edu/primerbank/>).**Table S5.** RT-qPCR cycle conditions.

Phase	T (°C)	Time (min)	Repetition
Denaturation	95 °C	2:00	
Denaturation	95 °C	0:05	
Annealing + Extension	60 °C	0:20	×40
Denaturation	95 °C	0:05	
Melting Curve	65-95 °C	18:00	

Evaluation of Cell Proliferation

It is often challenging to detach cells from the MCs on which they grew quantitatively. For this reason, we developed a protocol based on nuclei count: A cell lysis buffer solution frees the nuclei that can thus be enumerated by flow cytometry. This method also allows assessing the cell cycle status of the collected nuclei. So, it is possible to determine the proliferative status of the cells grown on the MCs.

Protocol: Nuclei count after cell lysis

- Collect the MCs + cells from each well and transfer them in 1.5 mL Eppendorf tubes. Rinse each well twice with PBS to recover all the MCs + cells.
- Centrifuge at 400 g for 5 min at RT.
- Discard the supernatant and resuspend the pellet (microcarriers + cells) in 1 mL of "Lysis & Nuclei Extraction Buffer" (LNEB; 0,2 M Citric acid + 2% Triton X-100).
- Incubate 5-10 min at RT and pipette up and down until the cells are completely lysed.
- Add the lysate to a pluriStrainer Mini 40 μ m inserted into a 5 mL Eppendorf tube (pluriSelect, cat. no. 43-10040-60, see figure S1). The strainer separates microcarriers from cell lysate/nuclei. Wash filters twice with LNEB to recover all the nuclei.
- Centrifuge at 800 g for 5 min at RT (5 mL Eppendorf + filter) to collect the nuclei.
- Resuspend the pellet (nuclei) in 100 μ L of CLNEB.
- Stain with 7-AAD for 5 min at RT and analyze by flow cytometry. Nuclei analysis: discrimination between G1, G2, and S phases.

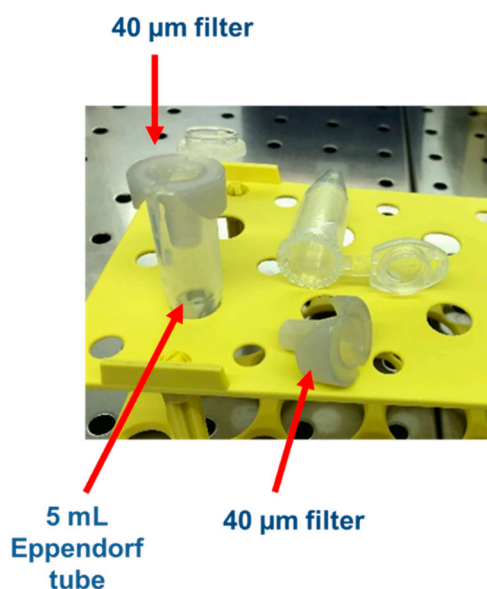


Figure S1. A pluriStrainer Mini 40 μ m is used to separate MCs from the nuclei. The centrifugal force helps to collect the nuclei quantitatively on the bottom of a 5 mL Eppendorf tube.

2. Supplementary Information for the Results Section

2.1. The Shape of Commercial MCs

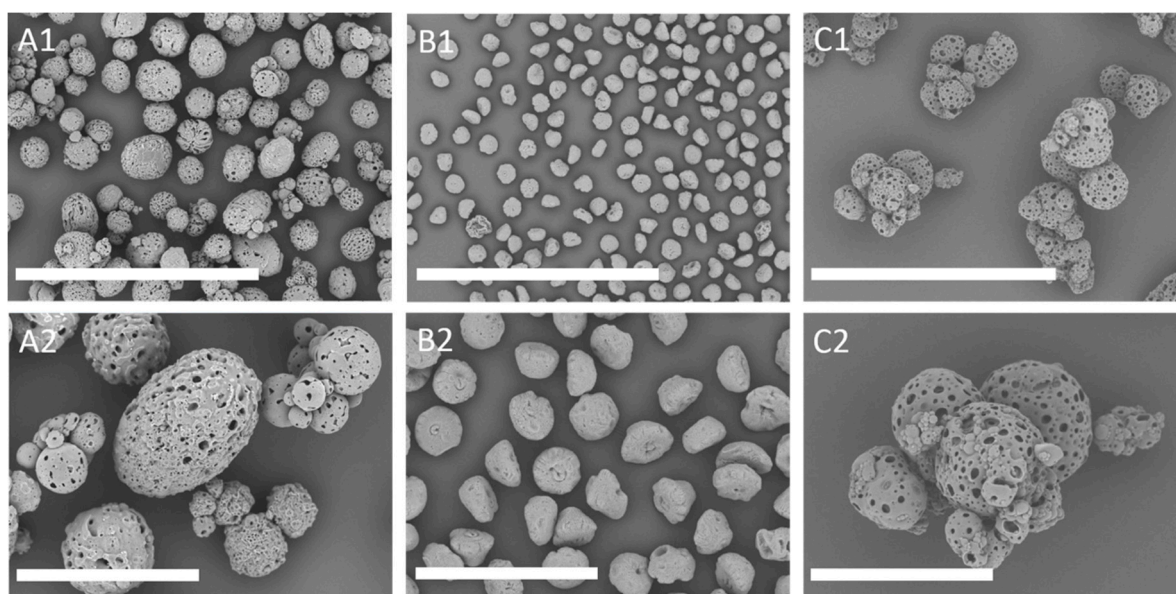


Figure S2. SEM microphotographs to show the morphology of some commercial dry MCs. (A1), (A2): Cultiphere G (Sigma, #M9418-10G); (B1), (B2): Corning dissolvable Synthemax II (Corning, #4988); (C1), (C2): Fujifilm, Injectable macroporous cell carrier (www.fujifilmcellmatrix.com). Magnification: (A1), (B1), (C1): 100X, scale bar 1 mm; (A2), (B2), (C2): 250X, scale bar 300 μm . Corning dissolvable Synthemax II MCs have a particular morphology that resembles a shell of a marine mollusk. However, after hydration, they are perfectly spherical and transparent (not shown).

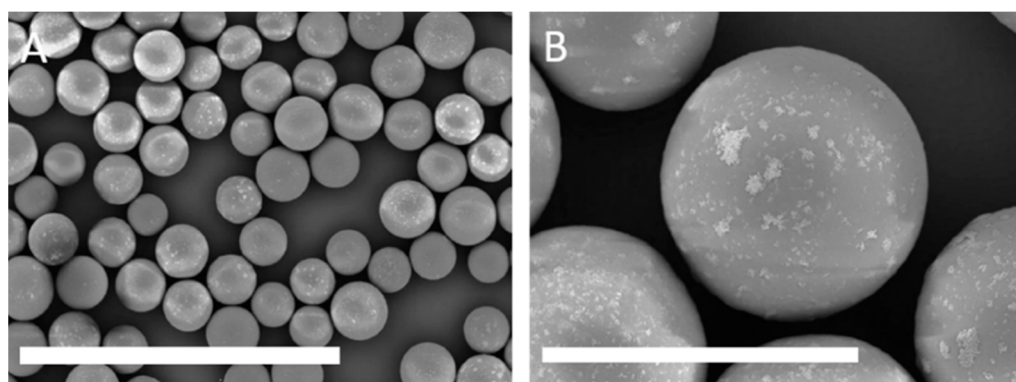


Figure S3. SEM images to show the morphology of ProNectin-F MCs. We used this carrier as a positive control for our tests. It consists of a synthetic core bead with a thin layer of recombinant, non-animal source polymer that incorporates multiple copies of the RGD attachment ligand of human fibronectin. The microphotographs show that the peptide-coating is not evenly distributed on the surface of the carriers. Magnification: (A): 100X, scale bar 1 mm; (B): 500X scale bar 200 μm .

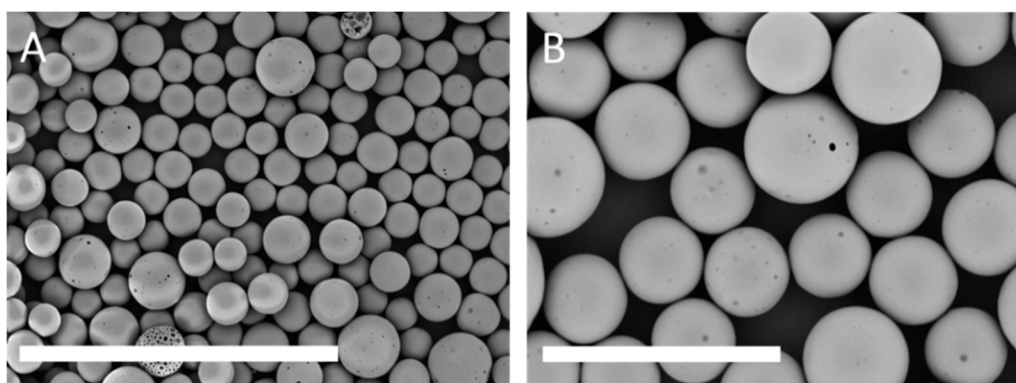


Figure S4. SEM microphotographs to show the morphology of the MC were used as a negative control. This carrier, named BR13, consists of only a mixture of poly lactic-co-glycolic acid (PLGA, no gelatin). This MC interact neither with the CF633 fluorescent dye nor with the ASC52telo cells. Magnifications: (A): 100X, scale bar 1 mm; (B): 250X, scale bar 300 μm .

2.2. Proof of Homogeneous Gelatin Distribution on MC Surface

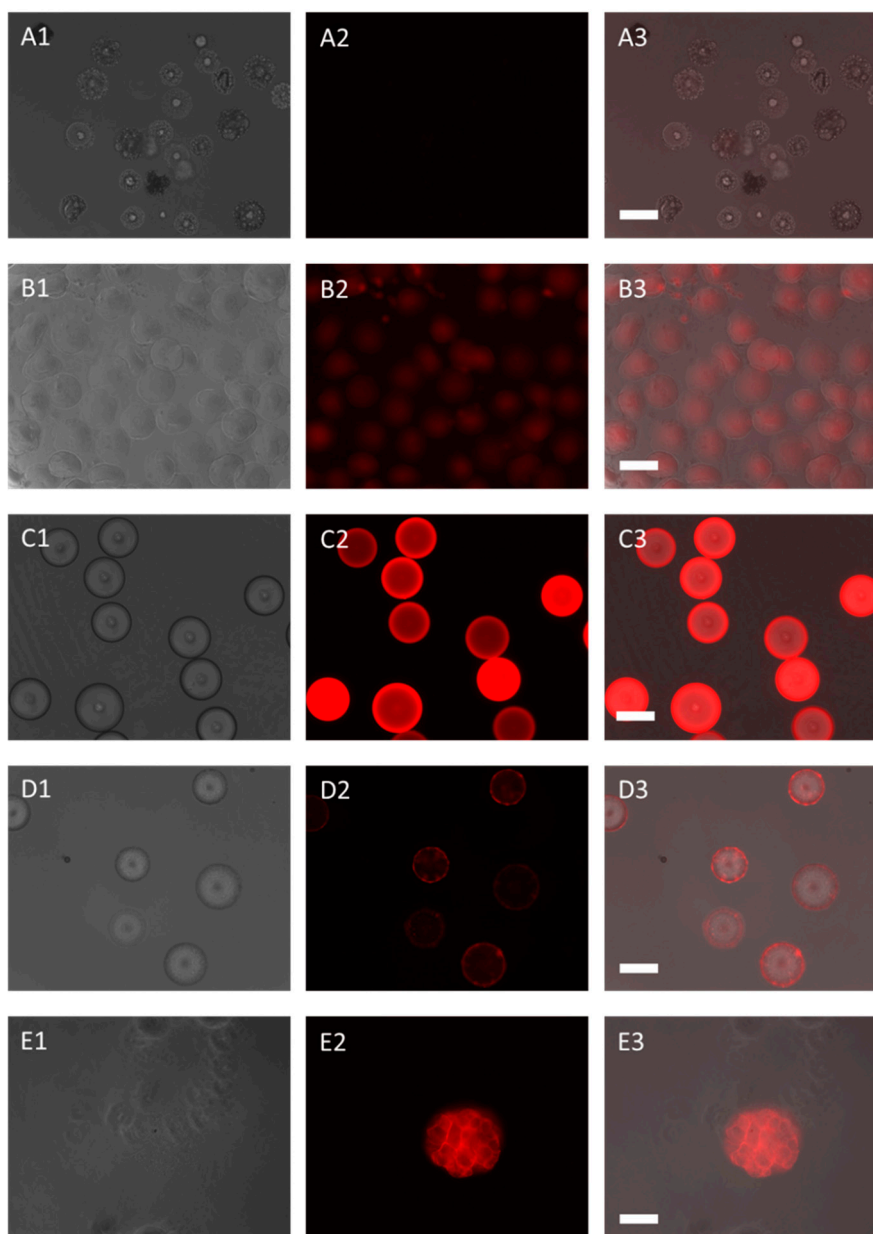


Figure S5. Fluorescent microphotographs of the MCs after reaction with the CF633 dye. Exposure time: 400 ms, except for (C1), (C2), and (C3) (80 ms). We chose as a negative control for this test the MC prototype BR13, which does not contain proteins and is made of pure PLGA. As a positive control, we used some commercial microcarriers with a reactive surface (primary amines, peptides) for the CF633 dye or a protein coating (Collagen I, Fibronectin, Gelatin) on their outer shell. (A.) BR13 (negative control). (B.) Corning Collagen I, #3786 (positive control). (C.) Corning Positive Charged Surface, #3787 (positive control). (D.) ProNectin-F (positive control). (E.) MC prototype BR44 (test MC). (1.) Bright-Field (2.) Fluorescence, red channels (3.) Merged. Magnifications: 100X, scale bar 150 μm .

It is interesting to note that the fluorescence shown by the carrier ProNectin-F is spotted. This observation agrees with the one made at the SEM, where it was noticed that the MC surface coating is not homogeneous (Figure S3). By contrast, the MC "Corning Positive Charge Surface" fluorescence is powerful and homogeneous. This suggests that the density for primary amines on its surface must be very high.

2.3. BR44 Stability under Stirred Conditions

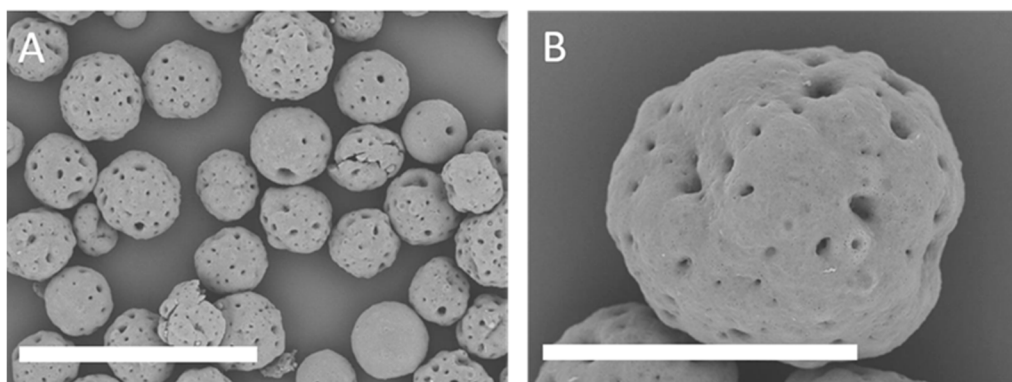


Figure S6. SEM microphotographs of the carrier BR44 after four days in culture without cells. The morphology changes, it seems to have been smoothed, and its pores shrink. This is a sign of its biodegradability. Magnifications: (A): 250X, scale bar 300 μm ; (B): 1000X, scale bar 100 μm .

2.4. Attachment and Growth of the ASC52telo on MC BR44 and MC ProNectin-F under Static Conditions

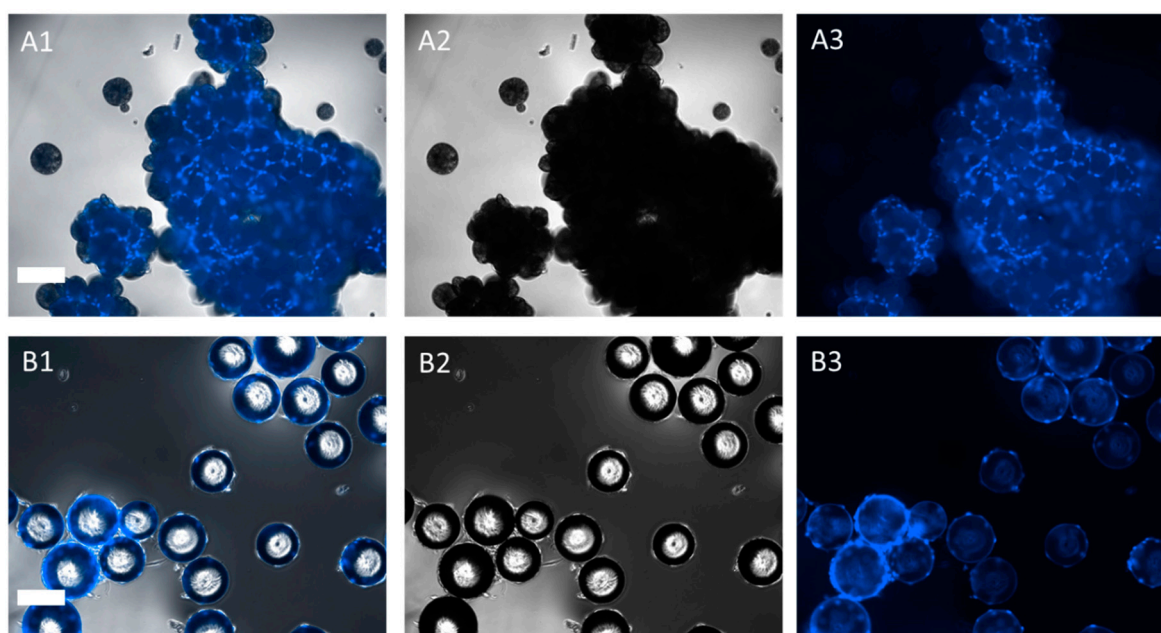


Figure S7. DAPI stained samples of ASCs52Telo cultured on the prototype MC BR44 and the commercial MC ProNectin-F in static condition for two days. (A) BR44, magnification 100X, scale bar 150 μm . (B) ProNectin-F, magnification 100X, scale bar 150 μm . (1) Merged (2) Bright-field (3) DAPI staining. The MC BR44 has the tendency, as the other MCs manufactured with biological polymers, to form larger aggregates than those generated by synthetic MCs like the MC ProNectin-F.

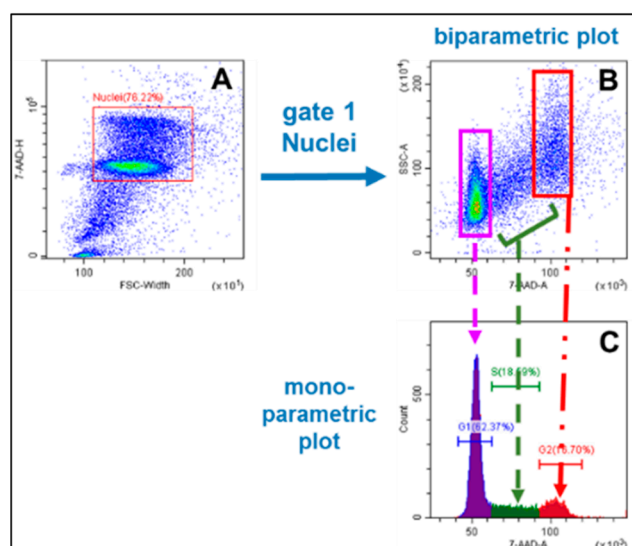


Figure S8. Analysis of nuclei released from the microcarrier-based culture of ASC52telo cells using 7-AAD and volumetric flow cytometry. Gating strategy for counting the nuclei: Debris was first excluded using forward side scatter (FSC) Width versus 7-AAD fluorescence intensity. The nuclei population was selected by defining the gate "Nuclei" (red rectangle in plot (A)). These selected events were further analyzed using 7-AAD fluorescence intensity versus side scatter (SSC, plot (B)). A monoparametric plot (C) of the 7-AAD-stained nuclei resolved those with a DNA content of 2N (first peak, G₀ and G₁ phases) and those with 4N (second peak, G₂ and M phases). Nuclei with an intermediate DNA content represent those in the S phase.

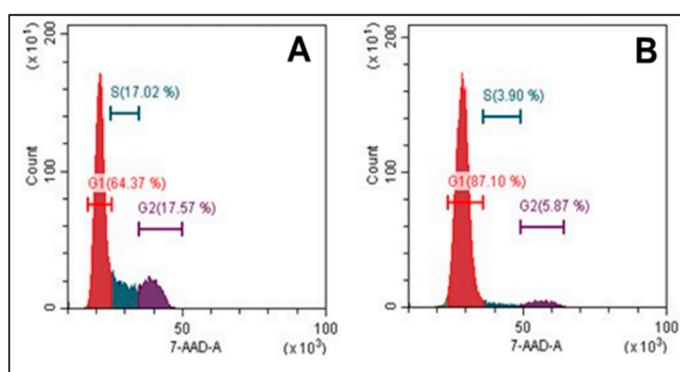


Figure S9. L-Mimosine stops proliferating ASC52telo cells before the onset of DNA replication. We used L-Mimosine to demonstrate that 7-AAD stained nuclei can provide information about the cells' cell cycle status under investigation. L-Mimosine inhibits the DNA replication, and, as shown in plot (B), the intensities of the S and the G2 peak are strongly reduced compared to untreated cells (plot (A)). The three peaks shown in plot A reflect the three major cell cycle stages of a cell population. The numerical quantification of the progression into the three cell cycle stages is possible by counting the number of events in each peak (G1, S and, G2).

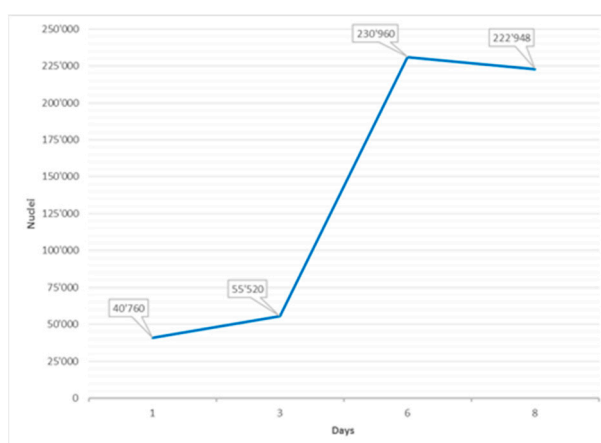


Figure S10. Growth curve: Graphical representation of the nuclei counts by flow cytometry of ASCs52Telo grown on MC BR44. The data are displayed according to the four daily measurements (day 1, 3, 6, and 8).

2.5. Calculation of Important Biochemical Engineering Parameters

(I) Impeller tip speed u_{tip} (Equation (1))

$$u_{tip} = \pi \cdot n \cdot d \tag{1}$$

where u_{tip} is the impeller tip speed, n and d are the impeller speed and the impeller diameter, respectively.

(II) Reynolds number Re (Equation (2))

$$Re = \frac{n \cdot d^2}{\nu} \tag{2}$$

where Re is the dimensionless Reynolds number, n and d are the impeller speed and the impeller diameter, and ν is the kinematic viscosity of the fluid.

(III) Specific power input P/V (Equation (3))

$$\frac{P}{V} = \frac{Ne \cdot \rho_l \cdot n^3 \cdot d^5}{V} \tag{3}$$

where P/V is the specific (volumetric) power input, Ne is the dimensionless Newton number, ρ_l , n and d are the density of the fluid, the impeller speed and the impeller diameter.

(IV) Local shear stress τ_{nt} (Equation (4))

$$\tau_{nt} = \sqrt{\left(\frac{\partial \tilde{w}_x}{\partial \tilde{y}} + \frac{\partial \tilde{w}_y}{\partial \tilde{x}}\right)^2 + \left(\frac{\partial \tilde{w}_x}{\partial \tilde{z}} + \frac{\partial \tilde{w}_z}{\partial \tilde{x}}\right)^2} \cdot \eta \tag{4}$$

where τ_{nt} is the local shear stress. Here, \tilde{w} are the velocities in the local coordinate systems defined by the coordinates \tilde{x} , \tilde{y} and \tilde{z} which are oriented along the fluid flow direction.

2.6. Proof-of-concept: Spinner Cultivation with BR44 and ProNectin-F MCs

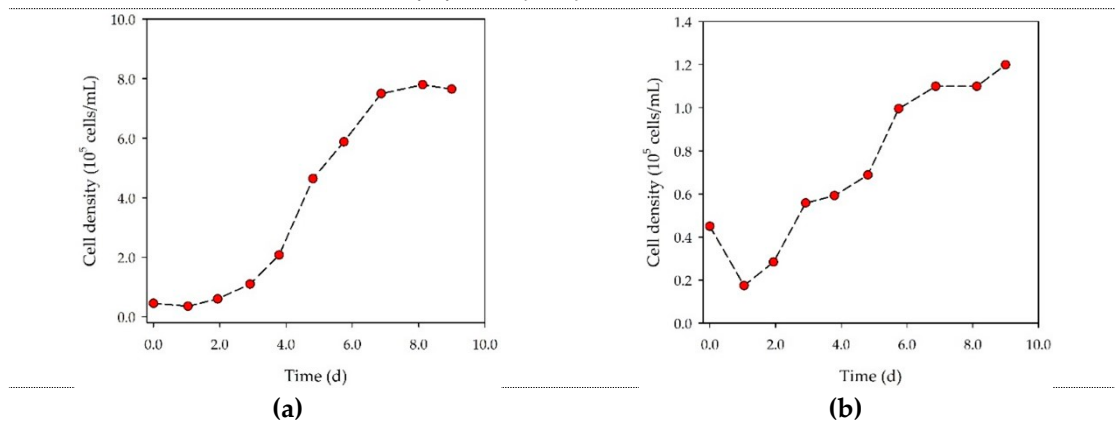


Figure S11. Time-dependent profiles of cell densities in the Corning spinner flasks. (a) ProNectin-F MCs, (b) BR44 MC. Partial medium exchanges of 50% were performed on days 4 and 8.

2.7. Cell Analytics: ASC52telo on BR44 MCs under Static Conditions

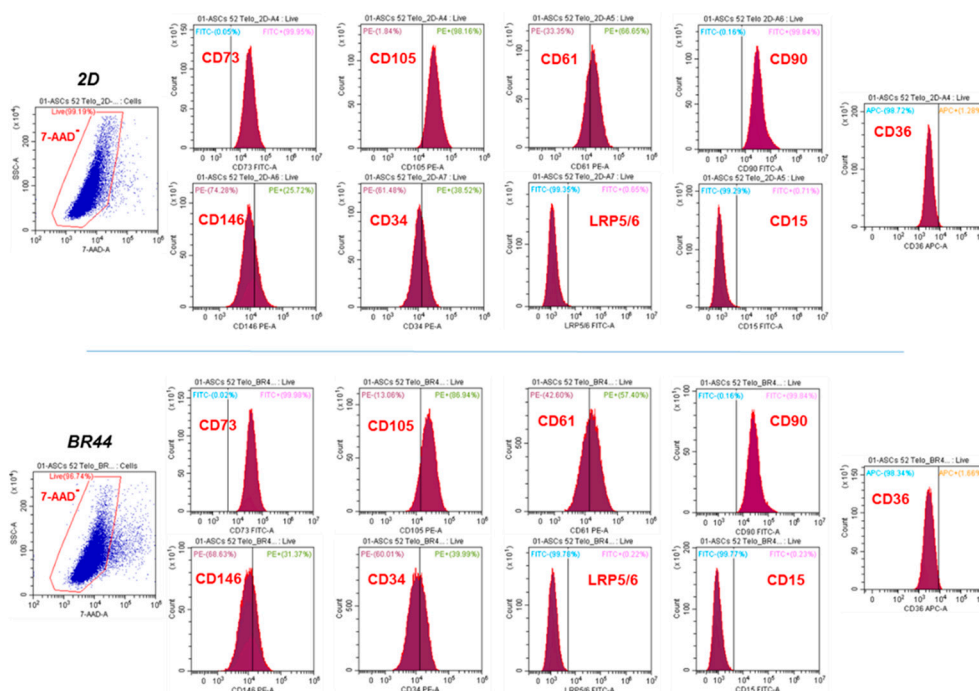


Figure S12. Single-parameter histograms for FACS analysis of known surface markers on AC52telo cells cultured in serum-free conditions (UrSuppe) on standard 2D cell culture vessels or microcarriers BR44 (3D). 7-AAD negative cells were checked for the expression of the nine indicated surface

markers. The cells were cultured in serum-free conditions in the standard cell culture vessels (2D, T25 flasks, upper panel) or on the microcarrier *BR44* (lower panel). Each plot's vertical axis marks the threshold "negative/positive" found with a sample of cells stained with the isotype control antibody. Therefore, the percentage of the population positive for each marker was calculated based on isotype controls stained cells.

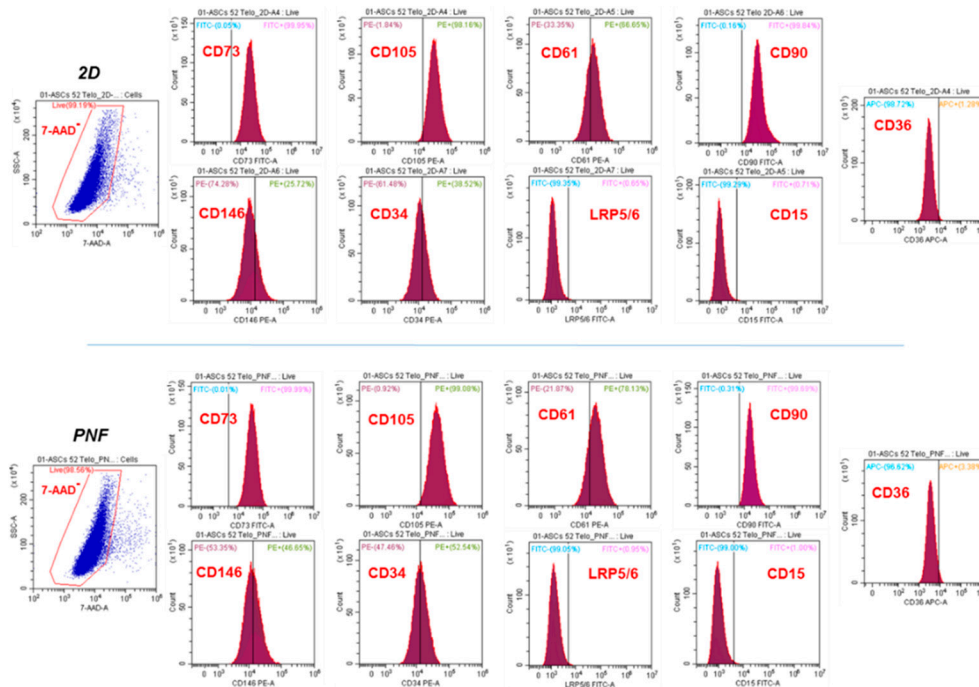


Figure S13. FACS analysis of known surface markers on AC52Telo cells cultured in serum-free conditions (UrSuppe): Comparison between cells grown on classical cell culture vessels (2D) or microcarriers ProNectin-F (PNF). 7-AAD negative cells were checked for the expression of the nine indicated surface markers. The cells were cultured in serum-free conditions in the standard cell culture vessels (2D, T25 flasks, upper panel) or on the commercial microcarrier ProNectin-F (lower panel). Each plot's vertical axis marks the threshold "negative/positive" found with a sample of cells stained with the isotype control antibody. Therefore, the percentage of the population positive for each marker was calculated based on isotype controls stained cells.

These FACS data suggest that, at least as far as concerning the markers examined, there are no major differences between cells grown in 2D from those grown in 3D on *BR44* or the microcarriers ProNectin-F. Maybe if one wants to be very meticulous, the percentage of CD146 positive cells is higher in ASC52telo cells grown on the MC ProNectin-F. The increased expression of this marker may be a negative indicator regarding the stemness. Indeed, CD146 is expressed by pre-adipocytes or other cells, such as pericytes [17,18]. CD34 is also usually expressed in more mature cells. [19–21]. The percentage of positive cells for this marker is also higher in ASC52telo grown on MC ProNectin-F.

2.8. Cell analytics: ASC52telo on *BR44* MCs under Dynamic Conditions

Tables S6 and S7 provide an overview and short description of genes measured in this study.

Table S6. Overview of measured stemness maintenance genes.

Name	Description	Reference
<i>PREF1 (DLK1)</i>	Pre-adipocyte factor 1 (Delta-like 1 homolog) is a transmembrane protein that inhibits adipogenesis, and it belongs to the non-canonical Notch ligands family.	Hudak et al. [22] Hei et al. [23]
<i>SOX9</i>	Sox9 is a member of the HMG-box class DNA-binding proteins and is a Pref1 target.	Wang and Sul [24]
<i>ZFP521</i>	Zinc Finger Protein 521 is a transcription factor, which inhibits adipogenesis.	Chiarella et al. [25] Kang et al. [16]
<i>WISP2</i>	Wnt1-inducible signaling pathway protein 2 is an endogenous and secreted auto/paracrine non-conventional WNT ligand.	Grünberg et al. [26] Hamardtedt et al. [27] Grünberg et al. [28]

Table S7. Overview of measured differentiation regulators/markers.

Name	Description	Reference
<i>PPARG</i>	Peroxisome Proliferator-Activated Receptor Gamma is a ligand-dependent transcription factor that is a member of the nuclear hormone receptor superfamily. It plays a crucial role in adipose tissue development and differentiation.	Ahmadian et al. [29] Barak et al. [30] Rosen et al. [31] Tontonoz et al. [32]
<i>ZFP423</i>	Zinc Finger Protein 423 is responsible for adipogenic commitment. It induces PPARG expression and terminal adipogenic differentiation.	Gupta et al. [33] Gupta et al. [34]
<i>DKK1</i>	Dickkopf1 inhibits the Wnt signaling and promotes differentiation.	Christodoulides et al. [35] Gustafson and Smith [36]
<i>RUNX2</i>	Runx2 is a transcription factor that is essential for osteoblast differentiation and chondrocyte maturation.	Komori [37] Komori [38]

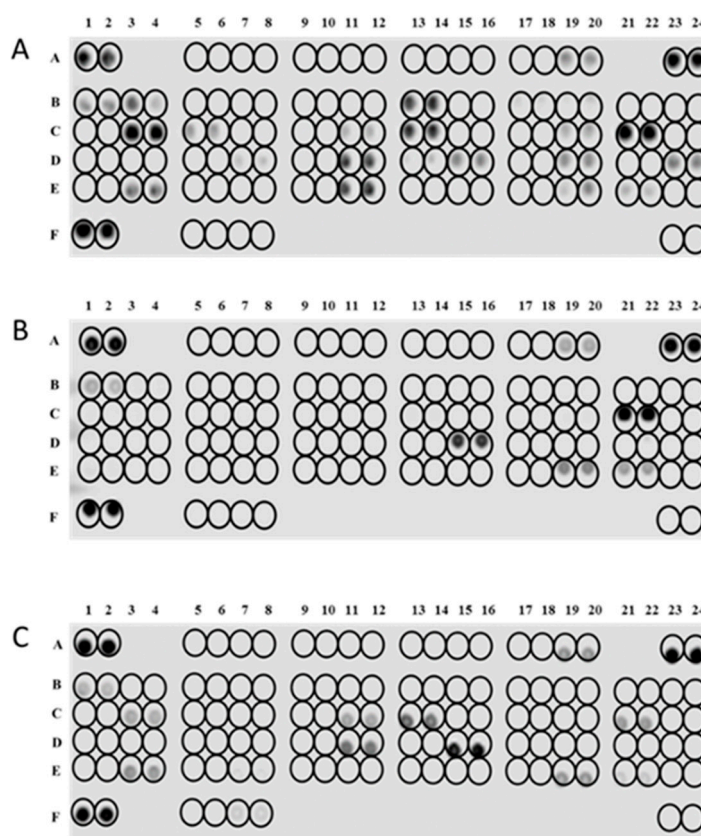


Figure S14. Comparing the adipokines secretion profile of ASC52telo cells. (A): Profile of ASC52telo cultured in the classical static 2D cell culture system. (B): Profile of ASC52telo cells grown on the microcarrier BR44 in a spinner flask. (C): Profile of ASC52telo cells grown on the microcarrier ProNectin-F in a spinner flask. Array procedure according to the manufacturer of the kit (biotechno, #ARY024).

Table S8. Human adipokine array.

Coordinate	Analyte/Control	Coordinate	Analyte/Control
A1, A2	Reference Spots	C19, C20	IL-6
A5, A6	Adiponectin/Acrp30	C21, C22	CXCL8/IL-8
A7, A8	Angiopoietin-1	C23, C24	IL-10
A9, A10	Angiopoietin-2	D1, D2	IL-11
A11, A12	Angiopoietin-like 2	D3, D4	LAP (TGF-β1)
A13, A14	Angiopoietin-like 3	D5, D6	Leptin
A15, A16	BAFF/BLyS/TNFSF13B	D7, D8	LIF
A17, A18	BMP-4	D9, D10	Lipocalin-2/NGAL
A19, A20	Cathepsin D	D11, D12	CCL2/MCP-1
A23, A24	Reference Spots	D13, D14	M-CSF
B1, B2	Cathepsin L	D15, D16	MIF
B3, B4	Cathepsin S	D17, D18	Myeloperoxidase
B5, B6	Chemerin	D19, D20	Nidogen-1/Entactin
B7, B8	Complement Factor D	D21, D22	Oncostatin M (OSM)
B9, B10	C-Reactive Protein/CRP	D23, D24	Pappalysin-1/PAPP-A

B11, B12	DPPIV/CD26	E1, E2	PBEF/Visfatin
B13, B14	Endocan	E3, E4	Pentraxin-3/SG-14
B15, B16	EN-RAGE	E5, E6	Pref-1/DLK-1/FA1
B17, B18	Fetuin B	E7, E8	Proprotein Convertase 9/PCSK9
B19, B20	FGF basic	E9, E10	RAGE
B21, B22	FGF-19	E11, E12	CCL5/RANTES
B23, B24	Fibrinogen	E13, E14	Resistin
C1, C2	Growth Hormone	E15, E16	Serpin A8/AGT
C3, C4	HGF	E17, E18	Serpin A12
C5, C6	ICAM-I/CD54	E19, E20	Serpin E1/PAI-1
C7, C8	IGFBP-2	E21, E22	TIMP-1
C9, C10	IGFBP-3	E23, E24	TIMP-3
C11, C12	IGFBP-4	F1, F2	Reference Spots
C13, C14	IGFBP-6	F5, F6	TNF- α
C15, C16	IGFBP-rp1/IGFBP-7	F7, F8	VEGF
C17, C18	IL-1 β /IL-1F2	F23, F24	Negative Controls

Table/List on the left: Coordinates and explanations of the 58 different spots present on the human adipokine array membrane.

Reference

1. Suarez Muñoz, M.; Confalonieri, D.; Walles, H.; van Dongen, E.M.W.M.; Dandekar, G. Recombinant Collagen I Peptide Microcarriers for Cell Expansion and Their Potential Use As Cell Delivery System in a Bioreactor Model. *J. Vis. Exp.* **2018**, doi:10.3791/57363.
2. Yan, X.; Zhang, K.; Yang, Y.; Deng, D.; Lyu, C.; Xu, H.; Liu, W.; Du, Y. Dispersible and Dissolvable Porous Microcarrier Tablets Enable Efficient Large-Scale Human Mesenchymal Stem Cell Expansion. *Tissue Eng. Part C Methods* **2020**, *26*, 263–275, doi:10.1089/ten.tec.2020.0039.
3. Rodrigues, A.L.; Rodrigues, C.A. V.; Gomes, A.R.; Vieira, S.F.; Badenes, S.M.; Diogo, M.M.; Cabral, J.M.S. Dissolvable Microcarriers Allow Scalable Expansion And Harvesting Of Human Induced Pluripotent Stem Cells Under Xeno-Free Conditions. *Biotechnol. J.* **2019**, *14*, 1800461, doi:10.1002/biot.201800461.
4. Santos, F. dos; Andrade, P.Z.; Abecasis, M.M.; Gimble, J.M.; Chase, L.G.; Campbell, A.M.; Boucher, S.; Vemuri, M.C.; Silva, C.L. da; Cabral, J.M.S. Toward a Clinical-Grade Expansion of Mesenchymal Stem Cells from Human Sources: A Microcarrier-Based Culture System Under Xeno-Free Conditions. *Tissue Eng. Part C Methods* **2011**, *17*, 1201–1210, doi:10.1089/ten.tec.2011.0255.
5. Rubin, J.P.; Bennett, J.M.; Doctor, J.S.; Tebbets, B.M.; Marra, K.G. Collagenous microbeads as a scaffold for tissue engineering with adipose-derived stem cells. *Plast. Reconstr. Surg.* **2007**, *120*, 414–424.
6. Rafiq, Q.A.; Coopman, K.; Nienow, A.W.; Hewitt, C.J. Systematic microcarrier screening and agitated culture conditions improves human mesenchymal stem cell yield in bioreactors. *Biotechnol. J.* **2016**, *11*, 473–486, doi:10.1002/biot.201400862.
7. Yuan, Y.; Kallos, M.S.; Hunter, C.; Sen, A. Improved expansion of human bone marrow-derived mesenchymal stem cells in microcarrier-based suspension culture. *J. Tissue Eng. Regen. Med.* **2014**, *8*, 210–225, doi:10.1002/term.1515.
8. Shekaran, A.; Lam, A.; Sim, E.; Jialing, L.; Jian, L.; Wen, J.T.P.; Chan, J.K.Y.; Choolani, M.; Reuveny, S.; Birch, W.; et al. Biodegradable ECM-coated PCL microcarriers support scalable human early MSC expansion and

- in vivo bone formation. *Cytotherapy* **2016**, *18*, 1332–1344.
9. Lam, A.T.L.; Li, J.; Toh, J.P.W.; Sim, E.J.H.; Chen, A.K.L.; Chan, J.K.Y.; Choolani, M.; Reuveny, S.; Birch, W.R.; Oh, S.K.W. Biodegradable poly- ϵ -caprolactone microcarriers for efficient production of human mesenchymal stromal cells and secreted cytokines in batch and fed-batch bioreactors. *Cytotherapy* **2017**, *19*, 419–432, doi:10.1016/j.jcyt.2016.11.009.
 10. Li, J.; Lam, A.T.L.; Toh, J.P.W.; Reuveny, S.; Oh, S.K.W.; Birch, W.R. Fabrication of uniform-sized poly- ϵ -caprolactone microspheres and their applications in human embryonic stem cell culture. *Biomed. Microdevices* **2015**, *17*, 105, doi:10.1007/s10544-015-0010-6.
 11. Li, J.; Lam, A.T.L.; Toh, J.P.W.; Reuveny, S.; Oh, S.K.W.; Birch, W.R. Tunable Volumetric Density and Porous Structure of Spherical Poly- ϵ -caprolactone Microcarriers, as Applied in Human Mesenchymal Stem Cell Expansion. *Langmuir* **2017**, *33*, 3068–3079, doi:10.1021/acs.langmuir.7b00125.
 12. Lee, Y.S.; Lim, K.S.; Oh, J.E.; Yoon, A.R.; Joo, W.S.; Kim, H.S.; Yun, C.O.; Kim, S.W. Development of porous PLGA/PEI1.8k biodegradable microspheres for the delivery of mesenchymal stem cells (MSCs). *J. Control. Release* **2015**, *205*, 128–133, doi:10.1016/j.jconrel.2015.01.004.
 13. Leber, J.; Barezai, J.; Blumenstock, M.; Pospisil, B.; Salzig, D.; Czermak, P. Microcarrier choice and bead-to-bead transfer for human mesenchymal stem cells in serum-containing and chemically defined media. *Process Biochem.* **2017**, *59*, 255–265, doi:10.1016/j.procbio.2017.03.017.
 14. Tan, K.Y.; Teo, K.L.; Lim, J.F.Y.; Chen, A.K.L.; Reuveny, S.; Oh, S.K. Serum-free media formulations are cell line-specific and require optimization for microcarrier culture. *Cytotherapy* **2015**, *17*, 1152–1165, doi:10.1016/j.jcyt.2015.05.001.
 15. Baki, A.; Rahman, C. V.; White, L.J.; Scurr, D.J.; Qutachi, O.; Shakesheff, K.M. Surface modification of PDLLGA microspheres with gelatine methacrylate: Evaluation of adsorption, entrapment, and oxygen plasma treatment approaches. *Acta Biomater.* **2017**, *53*, 450–459, doi:10.1016/j.actbio.2017.01.042.
 16. Kang, S.; Akerblad, P.; Kiviranta, R.; Gupta, R.K.; Kajimura, S.; Griffin, M.J.; Min, J.; Baron, R.; Rosen, E.D. Regulation of Early Adipose Commitment by Zfp521. *PLoS Biol.* **2012**, *10*, doi:10.1371/journal.pbio.1001433.
 17. Leroyer, A.S.; Blin, M.G.; Bachelier, R.; Bardin, N.; Blot-Chabaud, M.; Dignat-George, F. CD146 (Cluster of Differentiation 146): An Adhesion Molecule Involved in Vessel Homeostasis. *Arterioscler. Thromb. Vasc. Biol.* **2019**, *39*, 1026–1033, doi:10.1161/ATVBAHA.119.312653.
 18. Walmsley, G.G.; Atashroo, D.A.; Maan, Z.N.; Hu, M.S.; Zielins, E.R.; Tsai, J.M.; Duscher, D.; Paik, K.; Tevlin, R.; Marecic, O.; et al. High-Throughput Screening of Surface Marker Expression on Undifferentiated and Differentiated Human Adipose-Derived Stromal Cells. *Tissue Eng. - Part A* **2015**, *21*, 2281–2291, doi:10.1089/ten.tea.2015.0039.
 19. Festy, F.; Hoareau, L.; Bes-Houtmann, S.; Péquin, A.M.; Gonthier, M.P.; Munstun, A.; Hoarau, J.J.; Césari, M.; Roche, R. Surface protein expression between human adipose tissue-derived stromal cells and mature adipocytes. *Histochem. Cell Biol.* **2005**, *124*, 113–121, doi:10.1007/s00418-005-0014-z.
 20. Sidney, L.E.; Branch, M.J.; Dunphy, S.E.; Dua, H.S.; Hopkinson, A. Concise Review: Evidence for CD34 as a Common Marker for Diverse Progenitors. *Stem Cells* **2014**, *32*, 1380–1389, doi:10.1002/stem.1661.
 21. Scherberich, A. A familiar stranger: CD34 expression and putative functions in SVF cells of adipose tissue. *World J. Stem Cells* **2013**, *5*, 1, doi:10.4252/wjsc.v5.i1.1.
 22. Hudak, C.S.; Gulyaeva, O.; Wang, Y.; Park, S. min; Lee, L.; Kang, C.; Sul, H.S. Pref-1 marks very early mesenchymal precursors required for adipose tissue development and expansion. *Cell Rep.* **2014**, *8*, 678–687, doi:10.1016/j.celrep.2014.06.060.

23. Hei, S.S. Minireview: Pref-1: Role in adipogenesis and mesenchymal cell fate. *Mol. Endocrinol.* **2009**, *23*, 1717–1725, doi:10.1210/me.2009-0160.
24. Wang, Y.; Sul, H.S. Pref-1 Regulates Mesenchymal Cell Commitment and Differentiation through Sox9. *Cell Metab.* **2009**, *9*, 287–302, doi:10.1016/j.cmet.2009.01.013.
25. Chiarella, E.; Aloisio, A.; Codispoti, B.; Nappo, G.; Scicchitano, S.; Lucchino, V.; Montalcini, Y.; Camarotti, A.; Galasso, O.; Greco, M.; et al. ZNF521 Has an Inhibitory Effect on the Adipogenic Differentiation of Human Adipose-Derived Mesenchymal Stem Cells. *Stem cell Rev. reports* **2018**, *14*, 901–914, doi:10.1007/s12015-018-9830-0.
26. Grünberg, J.R.; Hammarstedt, A.; Hedjazifar, S.; Smith, U. The novel secreted adipokine wnt1-inducible signaling pathway protein 2 (WISP2) is a mesenchymal cell activator of canonical WNT. *J. Biol. Chem.* **2014**, *289*, 6899–6907, doi:10.1074/jbc.M113.511964.
27. Hammarstedt, A.; Hedjazifar, S.; Jenndahl, L.; Gogg, S.; Grunberg, J.; Gustafson, B.; Klimcakova, E.; Stich, V.; Langin, D.; Laakso, M.; et al. WISP2 regulates preadipocyte commitment and PPAR γ activation by BMP4. *Proc. Natl. Acad. Sci. U. S. A.* **2013**, *110*, 2563–2568, doi:10.1073/pnas.1211255110.
28. Grünberg, J.R.; Elvin, J.; Paul, A.; Hedjazifar, S.; Hammarstedt, A.; Smith, U. CCN5/WISP2 and metabolic diseases. *J. Cell Commun. Signal.* **2018**, *12*, 309–318, doi:10.1007/s12079-017-0437-z.
29. Ahmadian, M.; Suh, J.M.; Hah, N.; Liddle, C.; Atkins, A.R.; Downes, M.; Evans, R.M. PPAR γ signaling and metabolism : the good , the bad and the future. *Nat. Med.* **2013**, *19*, 557–566, doi:10.1038/nm.3159.
30. Barak, Y.; Nelson, M.C.; Ong, E.S.; Jones, Y.Z.; Ruiz-Lozano, P.; Chien, K.R.; Koder, A.; Evans, R.M. PPAR γ is required for placental, cardiac, and adipose tissue development. *Mol. Cell* **1999**, *4*, 585–595, doi:10.1016/S1097-2765(00)80209-9.
31. Rosen, E.D.; Sarraf, P.; Troy, A.E.; Bradwin, G.; Moore, K.; Milstone, D.S.; Spiegelman, B.M.; Mortensen, R.M. PPAR γ is required for the differentiation of adipose tissue in vivo and in vitro. *Mol. Cell* **1999**, *4*, 611–617, doi:10.1016/S1097-2765(00)80211-7.
32. Tontonoz, P.; Hu, E.; Spiegelman, B.M. Stimulation of adipogenesis in fibroblasts by PPAR γ 2, a lipid-activated transcription factor. *Cell* **1994**, *79*, 1147–1156, doi:10.1016/0092-8674(94)90006-X.
33. Gupta, R.K.; Arany, Z.; Seale, P.; Mepani, R.J.; Ye, L.; Conroe, H.M.; Roby, Y.A.; Kulaga, H.; Reed, R.R.; Spiegelman, B.M. Transcriptional control of preadipocyte determination by Zfp423. *Nature* **2010**, *464*, 619–623, doi:10.1038/nature08816.
34. Gupta Rana K. et al. Zfp423 expression identifies committed preadipocytes and localizes to adipose endothelial and perivascular cells. *Cell Metab.* **2012**, *15*, 230–239, doi:10.1016/j.cmet.2012.01.010.
35. Christodoulides, C.; Laudes, M.; Cawthorn, W.P.; Schinner, S.; Soos, M.; O'Rahilly, S.; Sethi, J.K.; Vidal-Puig, A. The Wnt antagonist Dickkopf-1 and its receptors are coordinately regulated during early human adipogenesis. *J. Cell Sci.* **2006**, *119*, 2613–2620, doi:10.1242/jcs.02975.
36. Gustafson D, B.; Smith, U. The WNT inhibitor dickkopf 1 and bone morphogenetic protein 4 rescue adipogenesis in hypertrophic obesity in humans. *Diabetes* **2012**, *61*, 1217–1224, doi:10.2337/db11-1419.
37. Toshihisa, K. Molecular Mechanism of Runx2-Dependent Bone Development. *Mol. Cells* **2020**, *43*, 168–175, doi:10.14348/molcells.2019.0244.
38. Komori, T. Runx2, an inducer of osteoblast and chondrocyte differentiation. *Histochem. Cell Biol.* **2018**, *149*, 313–323, doi:10.1007/s00418-018-1640-6.